Messenger-Tagging Electrosprayed Ions: Vibrational Spectroscopy of Suberate Dianions

Daniel J. Goebbert,† Torsten Wende, Risshu Bergmann, Gerard Meijer, and Knut R. Asmis*

Fritz-Haber-Institut der Max-Planck-Gesellschaft, Faradayweg 4-6, 14195 Berlin, Germany

Received: October 23, 2008; Revised Manuscript Received: February 26, 2009

The gas-phase vibrational spectroscopy of bare and monohydrated suberate dianions, $^{-}OOC-(CH_2)_6-COO^{-}$ and $^{-}OOC-(CH_2)_6-COO^{-}\cdot H_2O$, is studied by infrared photodissociation aided by electronic structure calculations. To this end, the corresponding ion−Kr atom complexes are formed in a cooled buffer-gas-filled ion trap, and their infrared vibrational predissociation spectra are measured in the range from 660 to 3600 cm^{-1}. The water molecule binds to one of the two carboxylate groups in a bidentate fashion, characterized by the splitting of the carboxylate stretching bands, a substantially blue-shifted water bending band, and the presence of anomalously broadened bands in the O−H stretching and H_2O rocking region. The C−C backbone structure remains unperturbed by the addition of a water molecule or a Kr atom. At 63 K, the all-trans isomer is the most abundant species, but evidence for dynamically interconverting conformers is also present from contributions to the absorption cross section on the low-energy tail of the C−H stretching region.

I. Introduction

Infrared photodissociation (IRPD) spectroscopy[1−9] has developed into a powerful and arguably one of the most sensitive, experimental tools to characterize the structure of ions in the gas phase. Direct photodissociation experiments[2,4,7−9] are nowadays often performed using the radiation from IR free electron lasers (FELs) and proceed via IR multiple photon dissociation. Commercially available, widely tunable IR lasers[10,11] exhibit a considerably narrower spectral bandwidth than FELs and thus allow, in principle, for a more detailed structural characterization. However, the photon flux produced by these tabletop lasers is generally not sufficient to induce direct photodissociation, and therefore, they are better suited for infrared vibrational predissociation spectroscopy methods,[1,3,5,6,12] which rely on the formation of more weakly bound complexes.

The use of electrospray sources in combination with tabletop IR lasers in PD experiments has been very limited (see, for example, refs 13 and 14 for exceptions) because of difficulties in the efficient production of the corresponding messenger complexes. Here, we make use of an alternative experimental scheme[15,16] which separates the ion production process from the ion−messenger atom complex formation process and thus represents a generally applicable strategy to study ions using IRPD spectroscopy of the corresponding ion−rare gas atom complex. As a model system, we use the suberate dianion $^{-}OOC-(CH_2)_6-COO^{-}$ (**1**) and the corresponding water complex $\mathbf{1}\cdot H_2O$. Microhydrated dicarboxylate dianions, in general, prove useful in studying of the hydrophobic and hydrophilic forces governing ion hydration at the molecular level, which is of particular interest in this case because **1** exhibits solvent-mediated folding.[17]

The present study is aimed at characterizing the gas-phase vibrational spectroscopy of the suberate dianion **1** and how the addition of a single water molecule effects its vibrational signature. On the basis of these results, a strategy for characterizing the solvent-mediated folding of **1** using infrared spectroscopy is developed. **1** and $\mathbf{1}\cdot H_2O$ are formed in an electrospray source, and the structure of the ions is studied by IRPD spectroscopy of the corresponding dianion−Kr atom complexes in combination with quantum chemical calculations.

II. Experimental Methods Section

The experimental setup is shown in Figure 1. Briefly, gas-phase anions are continuously produced in a commercial Z-spray source from a 3×10^{-3} M solution of suberic acid in a 80/20 water/acetonitrile mixture. The beam of negative ions passes through a 4 mm diameter skimmer and is then collimated in a radio frequency (RF) decapole ion guide. Parent ions are mass-selected in a quadrupole mass filter, deflected by 90° in an electrostatic quadrupole deflector, and focused into a gas-filled RF ring electrode ion trap. To allow for continuous ion loading, ion thermalization, and ion−Kr atom complex formation, the trap is continuously filled with a buffer gas of 1% Kr in He (∼0.01 mbar) at an ion trap temperature of 63 K. At lower ion trap temperatures, the Kr gas condenses on the ion trap electrodes, while at higher temperatures, complex formation is less efficient. After filling the trap for 95 ms (195 ms @ 5 Hz), all ions are extracted from the ion trap and focused both temporally and spatially into the center of the extraction region of an orthogonally mounted linear time-of-flight (TOF) mass spectrometer. Here, they interact with the IR laser pulse, either from a Laservision OPO/OPA IR laser (2775−3600 cm^{-1}) or the free-electron laser for infrared experiments FELIX (660−1775 cm^{-1}) at the FOM-Institute for Plasma Physics Rijnhuizen.[18] The tabletop laser produces 7 ns/15 mJ pulses at 10 Hz with a spectral bandwidth of 2−3 cm^{-1} and is used for the absorption experiments in the C−H and O−H stretching region. FELIX is used to probe the fingerprint region and operated with 5 μs/25 mJ macropulses at 5 Hz with a spectral bandwidth of roughly 0.2% rms of the central wavelength. Finally, multiple photon absorption experiments of the bare ions (without Kr-tagging) in the C−H stretching region are also performed using FELIX lasing on its third harmonic (∼6 mJ @ 2900 cm^{-1}).

The timing between extraction of the ions from the ion trap, extraction of the ions into the TOF, and firing of the IR laser is

* To whom correspondence should be addressed. E-mail: asmis@fhi-berlin.mpg.de.
† Present address: Department of Chemistry, University of Arizona, Tucson, Arizona 85721-0041.

10.1021/jp809390x CCC: $40.75
Published on Web 04/24/2009

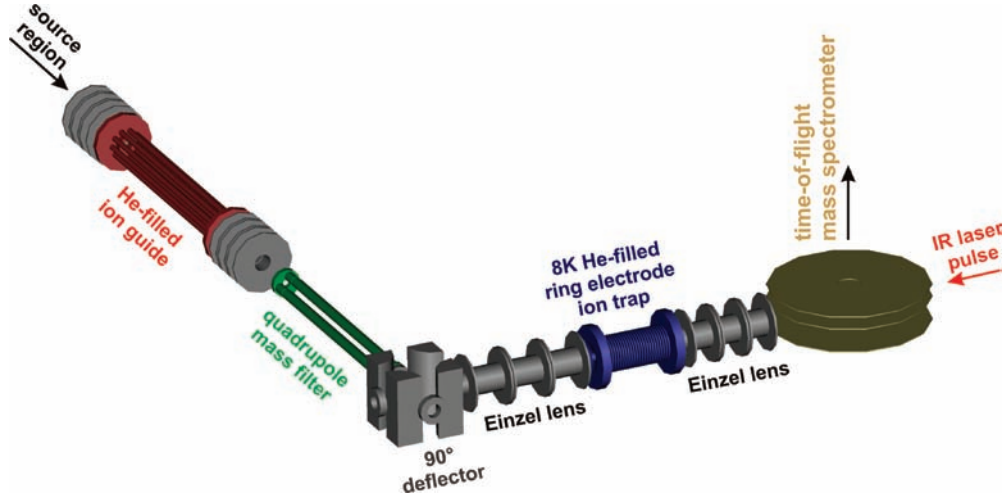

Figure 1. Schematic of the tandem mass spectrometer used in the present study. The continuous beam of negative ions from an electrospray source is collimated in a RF ion guide and mass-selected in a RF quadrupole mass filter. Mass-selected ions are deflected by 90° and continuously loaded into the buffer-gas-filled ring electrode ion trap held at 63 K. Dianion−Kr complexes are formed by three-body collisions with the buffer gas. After 95 ms, all ions are extracted from the ion trap and focused into the extraction region of an orthogonally mounted TOF mass spectrometer. Here, the ions interact with the IR photodissociation laser pulse, and the depletion of the parent ions, as well as the formation of photofragment ions, is monitored by way of TOF mass spectrometry.

optimized for maximum photodissociation signal. After laser irradiation, TOF mass spectra are measured by applying fast rise time (∼60 ns) high-voltage pulses (∼1500 V) to the extraction plates and monitoring the arrival time distribution 50 cm downstream using a 40 mm diameter dual microchannel plate detector in a chevron configuration. The output from the MCP is amplified and sent into a 100 MHz/12 bit digitizer for recording of the transient waveforms.

Geometry optimizations and harmonic frequency calculations are performed with the Gaussian 03 program package[19] using second-order perturbation theory (MP2) combined with the aug-cc-pVDZ basis set. Relative energies are corrected for zero-point energies, and the basis set superposition error is estimated using the counterpoise corrections for determining dissociation energies. Simulated linear absorption spectra are derived from MP2/aug-cc-pVDZ scaled harmonic frequencies (scaling factor: 0.959)[20] and intensities. The resulting stick spectra are convoluted using a Gaussian line shape function with a width of 10 cm^{-1} (fwhm).

III. Results and Discussion

III.A. Mass Spectrometry. The three mass spectra shown in Figure 2 reflect the ion distribution at different stages of the experiment. The quadrupole mass spectrum (i) in Figure 2 directly probes the distribution of ions produced by the electrospray source. The peaks at mass-to-charge ratios m/z (m: mass in amu; z: charge number) of 86.0, 95.0, and 104.0 amu are assigned to the suberate dianion **1** (m = 172 amu; z = 2) and the corresponding complexes with one and two water molecules. These water molecules, however, are not used as messenger species in the following photodissociation experiments because they are bound too strongly to the dianion (see below). Rare gas atoms are a better choice, and Kr atoms are used in the present experiments. In principle, He atoms would represent the ideal messenger atoms, but binding of rare gas atoms to negative ions is weaker than that to cations because the additional electrons in negative ions lead to increased electron repulsion and thus a more diffuse electron distribution. To compensate for this effect, rare gas atoms with larger polarizability are required for anions under the present experimental conditions.

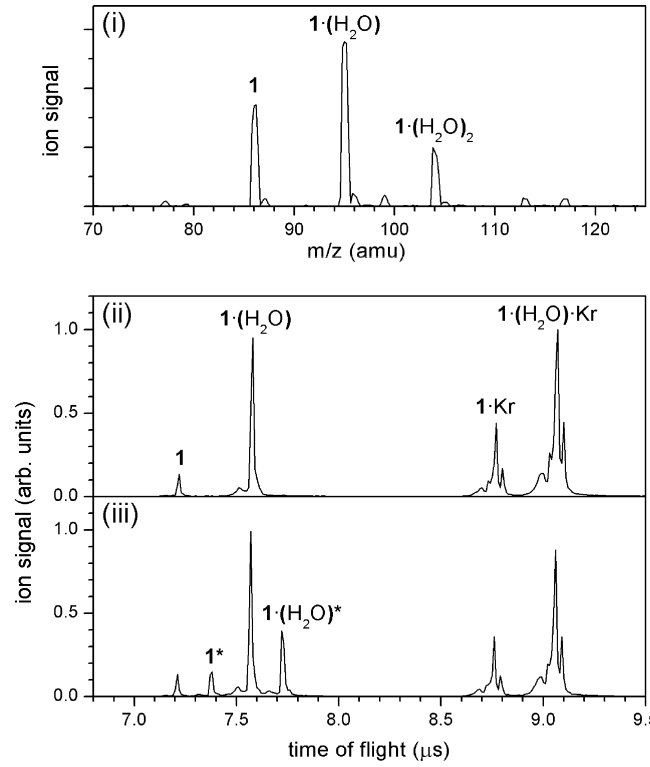

Figure 2. Quadrupole (trace i) and TOF (traces ii and iii) mass spectra. Trace (i) probes the distribution of doubly negatively charged ions produced by the electrospray source. Trace (ii) is measured with the quadrupole mass filter set to the mass-to-charge ratio of **1**·(H_2O) and reflects the distribution of ions extracted from the ion trap. Trace (iii) was measured with the IR laser set on resonance (2925 cm^{-1}). Triggering the laser pulse shortly after the high-voltage pulses have been applied to the TOF extraction plates allows for a background-free measurement of the IR photodissociation signal (see peaks at 7.38 and 7.72 μs).

For the IRPD experiments, mass-selected **1**·(H_2O) dianions are continuously trapped for 95 ms in the ion trap containing a 1% Kr in He gas mixture and kept at a temperature of 63 K. The TOF mass spectrum (ii) in Figure 2 measures the ion distribution after extracting all ions from the ion trap into the

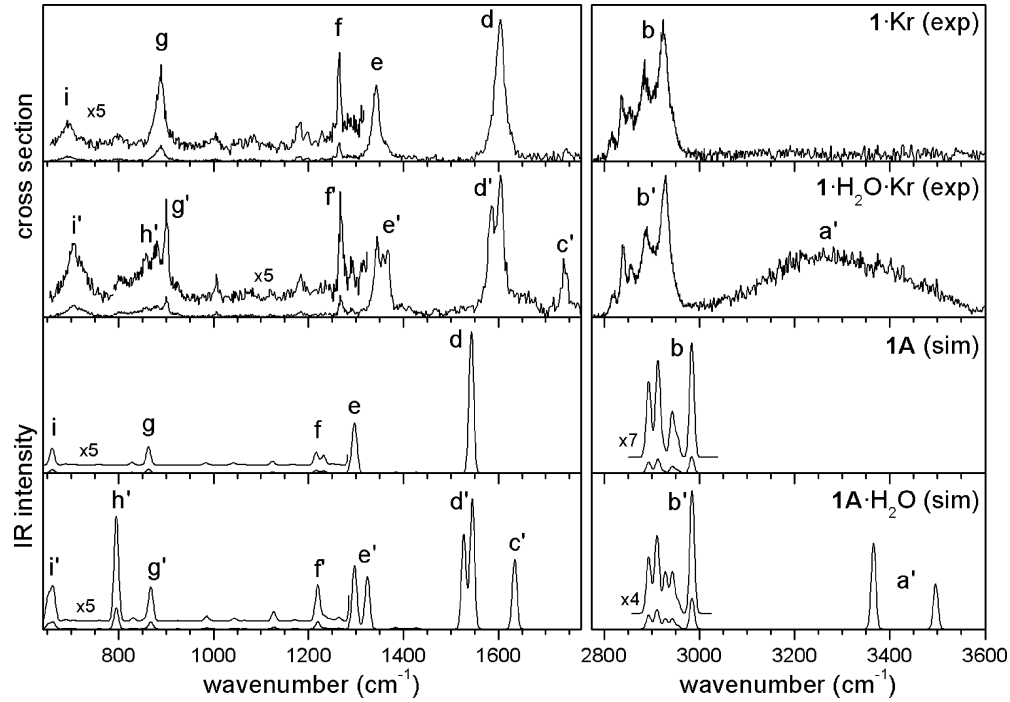

Figure 3. Top: IRPD spectra of the Kr-tagged suberate dianion (**1**·Kr) and the corresponding monohydrated dianion (**1**·H_2O·Kr) from 660 to 1775 and 2775 to 3600 cm^{-1}, measured simultaneously by monitoring the corresponding Kr atom loss channels as a function of the IR photon energy. Bottom: Simulated linear absorption spectra of **1A** and **1A**·H_2O, derived from MP2/aug-cc-pVDZ scaled (0.959) harmonic frequencies and intensities and convoluted using a Gaussian line shape function with a width of 10 cm^{-1} (fwhm).

TOF mass spectrometer. The mass-selected parent ion peak **1**·(H_2O) is observed at 7.58 μs. Under the present experimental conditions some of the ions entering the trap undergo collision-induced dissociation, forming the bare dianion **1** (7.22 μs). Both dianions, **1** and **1**·(H_2O), can also undergo three-body collisions involving a Kr atom, forming the corresponding Kr complexes **1**·Kr and **1**·(H_2O)·Kr, observed at ~8.8 and ~9.1 μs, respectively. These bands consists of multiple peaks and reflect the natural isotope distribution of Kr.

To measure IRPD spectra, ions extracted from the ion trap are irradiated by the IR laser pulse inside of the TOF mass spectrometer. When on resonance with an IR-active vibrational transition, this leads to vibrational predissociation of the Kr-tagged species because the photon energy used in the present experiments is sufficient to break the dianion−Kr bond. Photodissociation of the water complexes, on the other hand, is not observed because the corresponding binding energies are considerably higher than the photon energy. The MP2 calculations yield 89 kJ/mol for the **1**·(H_2O) → **1** + H_2O dissociation energy, which corresponds to 7440 cm^{-1} or 3−12 times the photon energy used in the present experiments.

Although messenger atom formation is accomplished under our experimental conditions, there remains a significant amount of unreacted ions **1** and **1**·(H_2O), as shown in (ii) of Figure 2. The presence of these ions contributes a background signal, and small fluctuations of these intense peaks would introduce unwanted noise in our IR spectra. In order to measure the photodissociation signal background-free, the IR laser pulse is applied 1 μs after the high-voltage pulses have been applied to the TOF extraction plates, that is, during the acceleration phase of the ions. The photodissociation signal then leads to additional peaks in the TOF mass spectra (iii) of Figure 2, labeled **1*** and **1**·(H_2O)*, which lie in between the corresponding parent (Kr-tagged species) and daughter ion (without Kr atom) peaks. Their exact position depends on the time delay between switching on the TOF voltages and firing the IR laser. In this way, IRPD spectra of **1**·Kr and **1**·(H_2O)·Kr can be measured background-free (and simultaneously).

III.B. Infrared Photodissociation Spectroscopy of Kr-Tagged Species. The experimental IRPD spectra of **1**·Kr and **1**·H_2O·Kr are shown in the top part of Figure 3. Peak positions and band assignments are listed in Table 1. The IRPD spectrum of **1**·Kr shows a broad, structured absorption band (labeled b in Figure 3) in the C−H stretching region, extending from 2800 to 2970 cm^{-1} with five characteristic maxima. A shoulder (~2940 cm^{-1}) is observed to the blue of the most intense absorption peak at 2925 cm^{-1}. The fwhm width of these peaks lies between 8 (2837 cm^{-1}) and 16 cm^{-1} (2925 cm^{-1}). The latter is considerably larger than expected, taking the laser bandwidth (~2−3 cm^{-1}) and the rotational band contour (~5−6 cm^{-1}) into account.

A C−H stretching band of nearly identical shape and position (b′ in Figure 3) is also observed for **1**·H_2O·Kr, indicating that the water molecule leaves the C−C backbone structure unperturbed and binds to one of the two carboxylate groups. A second absorption feature (a′) lies in the O−H stretching region but is unusually broad and shows no structure. A similarly broad band is observed in the IRPD spectrum of CH_3COO^-·H_2O·Ar, where the pronounced broadening was attributed to strong anharmonic coupling between the OH stretching modes and intermolecular rocking motion, characteristic of a bidentate binding motif of the water molecule to the carboxylate group.[21,22] Our spectra suggest that a similar coupling mechanism and thus a similar binding motif is present in **1**·H_2O·Kr.

The IRPD spectra of **1**·Kr and **1**·H_2O·Kr in the fingerprint region are shown in the left part of Figure 3. The spectrum of **1**·Kr is characterized by five bands at 1604 (d), 1343 (e), 1265 (f), 890 (g), and 697 cm^{-1} (i), as well as some smaller features. The two most intense bands (d and e) are assigned to the stretching modes of the carboxylate groups, which are generally

TABLE 1: Peak Positions (in cm^{-1}) and Band Assignments for the IRPD Spectra of the Suberate Dianion−Kr Complex (1·Kr) and the Suberate Dianion−H_2O−Kr Complex (1·H_2O·Kr) Shown in Figure 3

1·Kr		1·H_2O·Kr		
band	peak positions	band	peak positions	assignment
a		a′	3570−3010	O−H stretch + H_2O rock
b	2925, 2884, 2855, 2837, 2818	b′	2930, 2891, 2856, 2840, 2823	C−H stretch
c		c′	1738	H−O−H bend
d	1604	d′	1604, 1586	O−C−O antisym. stretch
e	1343	e′	1367, 1356, 1345	O−C−O sym. stretch, CH_2 wag
f	1265	f′	1267	CH_2 wag and twist
g	890	g′	901	C−C stretch/O−C−O bend
h		h′	890−820	H_2O rock + O−H stretch
i	697	i′	703	CH_2 rock/O−C−O bend

found in between 1550 and 1610 cm^{-1} (antisymmetric stretch) and 1300 and 1420 cm^{-1} (symmetric stretch).[23] Note, the two carboxylate groups yield four stretching modes, namely, a symmetric and an antisymmetric combination for the two types of carboxylate stretching modes, respectively. Bands d and e are somewhat broader than the laser bandwidth, indicating that the coupling between the two carboxylate groups is sufficient to broaden the peaks but too small to lead to a detectable splitting of these antisymmetric and symmetric combinations.

Compared to **1**·Kr, five bands of similar shape and relative intensity (d′, e′, f′, g′, and i′) are also observed in the IRPD spectrum of **1**·H_2O·Kr (see Figure 3 and Table 1), suggesting that they are of similar nature. All additionally observed features can then be attributed to the presence of the water molecule. First, the band at 1738 cm^{-1} (c′) corresponds to the water bending mode. It is well blue shifted from the free H−O−H bending frequency of 1595 cm^{-1}.[24] A similarly blue-shifted band is observed in the IR spectrum of NO_2^-·H_2O (∼1710 cm^{-1}),[25] yielding additional support for the bidentate binding motif of the water molecule to the carboxylate group. Second, the broad feature observed in between 820 and 890 cm^{-1} (h′) is tentatively assigned to the water rocking mode. As we assume that this intermolecular mode is strongly coupled to the intramolecular O−H stretching modes (see above), one expects a broadened feature similar to band a′. Third, the bands that correspond to the carboxylate stretches (d′ and e′) are split into multiple peaks. Binding of the water molecule to a single carboxylate group leads to a shift of the associated carboxylate stretching modes, while the two corresponding modes of the "free" carboxylate group remain unchanged. Interestingly, this shift is toward the red for the antisymmetric stretching mode (d′ versus d), while it is toward the blue for the symmetric stretching mode (e′ versus e).

III.C. Infrared Photodissociation Spectroscopy without Kr-Tagging. In order to study the influence of the H_2O and Kr ligands on the backbone structure of **1**, we measured the vibrational spectra of **1**·H_2O and **1**·$(H_2O)_2$ without an attached rare gas atom, using the water molecule as the messenger species. These experiments require the absorption of several IR photons and were therefore performed using FEL radiation. In order to probe the region above 2400 cm^{-1} with FELIX, third-harmonic radiation is required, making these experiments rather challenging, and we therefore restricted our efforts to study the C−H stretching region. These spectra are compared to those of **1**·Kr and **1**·H_2O·Kr in Figure 4. The spectra have been aligned to the maximum of the main absorption peak of trace (i) for better comparability, that is, spectra (ii)−(iv) were shifted by −3, +7 and +7 cm^{-1}, respectively. All four spectra look very similar, indicating that all ligands (Kr atoms as well as H_2O molecules) bind to either of the carboxylate groups without a significant perturbation of the C−C backbone structure, independent if one or two ligands are attached. Note, the substantial width of the observed peaks is independent of the radiation source used and therefore is not determined by the laser spectral bandwidth. Addition of the first water molecule leads to a small blue shift of all C−H stretching features by +3 cm^{-1}. Addition of a second water molecule has no further influence on the peak positions. The calibration for the spectra is not sufficiently accurate to determine the shift induced by the addition of a Kr atom to **1**·H_2O.

III.D. Simulated Infrared Absorption Spectra. In order to gain a more detailed understanding of the geometric structure of **1** and **1**·H_2O, we performed MP2/aug-cc-pVDZ calculations. The lowest-energy structure found for **1** is the all-trans isomer **1A** (see Scheme 1), previously reported in refs 17 and 26. Simulated linear absorption spectra of **1A** and **1A**·H_2O are shown in the bottom part of Figure 3. The simulated spectra reproduce the experimental spectra sufficiently well to assign all of the characteristic features. Some discrepancies remain with regard to the position and the relative intensity of the absorption bands. The empirical scaling factor 0.959 from ref 20 for the MP2/aug-cc-pVDZ harmonic frequencies leads to too high C−H

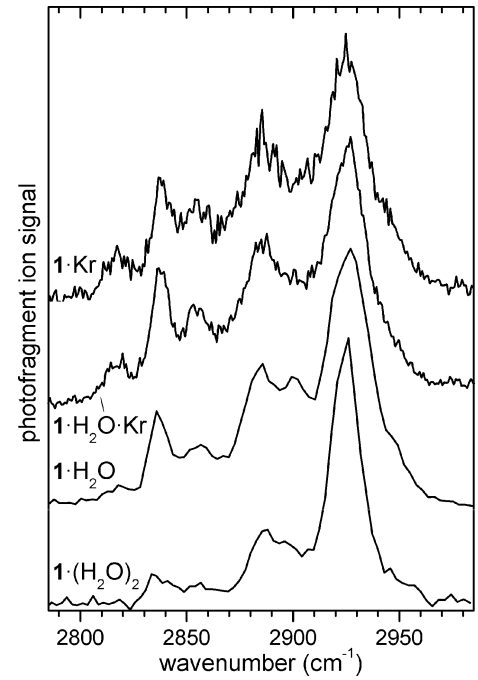

Figure 4. Comparison of the IRPD spectra of **1**·Kr, **1**·H_2O·Kr, **1**·H_2O, and **1**·$(H_2O)_2$ in the C−H stretching region. The spectra were measured by monitoring either the Kr atom loss (top two traces) or the H_2O loss channel (bottom two traces). The lower three spectra were shifted by −3, +7, and +7 cm^{-1}, respectively, to allow for a better comparison (see text).

SCHEME 1: Low-Energy Conformers of the Suberate Dianion (1) and Its Complex with Water

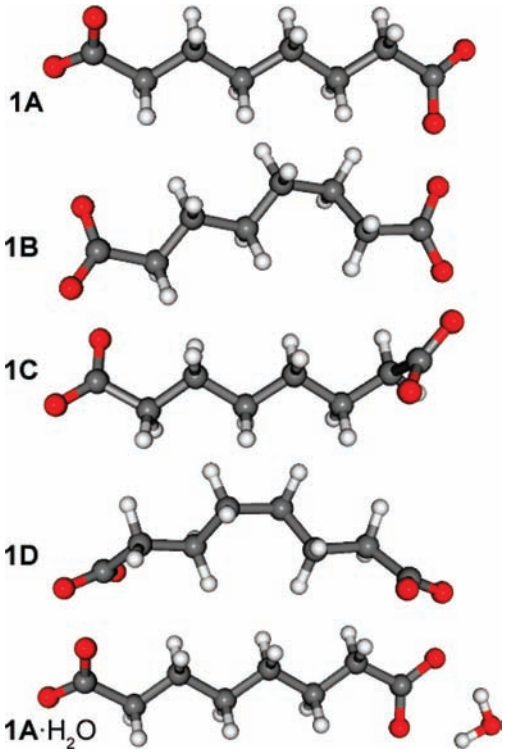

stretching frequencies (~+2%) and too low frequencies below 1800 cm^{-1} (−4%). The application of two separate scaling factors (0.94 and 1.0) improves the agreement, suggesting that the anharmonicities are substantially larger for the O−H and C−H stretching modes than those for the modes in the fingerprint region. The shape and position of the features a′ and h′, which are governed by anharmonic coupling effects, are expectedly not well reproduced by our simulations. In order to recover these effects, multidimensional calculations are required, which are beyond the scope of this work.

The simulated spectra capture the main features in the C−H stretching region. However, the relative intensities are different, and the lowest-energy C−H stretching absorption band at 2818 cm^{-1}, as well as the shoulder at 2940 cm^{-1}, is not reproduced. In more detail, the 12 C−H bonds in **1** combine to yield 12 C−H stretch normal modes, of which 7 are predicted to have sizable intensities (>10 km/mol). Combinations involving the antisymmetric (symmetric) CH_2 stretches are predicted above (below) 2913 cm^{-1}. The most intense vibrational mode is calculated at the highest energy (2984 cm^{-1}) and corresponds to a combination of six antisymmetric CH_2 stretches, in which adjacent CH_2 units oscillate out-of-phase. The calculations also confirm that the presence of a water molecule in **1A**·H_2O does not perturb the C−H stretching absorption region substantially.

In the region below 1800 cm^{-1}, the simulations confirm our initial assignments. Band d is due to the excitation of the antisymmetric stretching modes involving the two carboxylate groups. These yield a symmetric and an antisymmetric combination (1543 cm^{-1}), which are calculated within 0.1 cm^{-1} of each other and both with sizable IR intensity. The corresponding combinations for the symmetric carboxylate stretching modes are also calculated quasi-degenerate in energy (1298 and 1300 cm^{-1}), but only the antisymmetric combination is predicted to have significant IR intensity (band e). However, a CH_2 wagging mode is calculated within 2 cm^{-1} of the symmetric carboxylate stretching modes and contributes roughly 1/3 of the intensity of band e. All other IR-active modes have considerably smaller intensities. Band f is mainly due to CH_2 wagging (1232 cm^{-1}) and twisting modes (1216 cm^{-1}). Bands g and i correspond to modes that involve the O−C−O bending motion with significant contributions from the terminal C−C stretching (g) and CH_2 rocking motion (i), respectively.

Several of the differences observed in the two experimental spectra in Figure 3 can be understood based on the comparison of the simulated spectra of **1A** and **1A**·H_2O. The experimentally observed shift of one of the two modes for each pair of carboxylate stretching modes (d′: −18 cm^{-1}; e′: +22 cm^{-1}) is well reproduced (d′: −17 cm^{-1}; e′: +26 cm^{-1}). For **1A**·H_2O, both combinations of the symmetric stretching modes as well as the CH_2 wagging mode are active, accounting for the three peaks observed for band e′ in the spectrum of **1**·H_2O·Kr. The water bending mode is observed 134 cm^{-1} above the carboxylate antisymmetric stretching modes; the calculations yield 90 cm^{-1}. Finally, the harmonic frequency of the water rocking mode is calculated in between bands g and i, suggesting that the broad feature h′ is in the right spectral region to be assigned to this mode, which is distorted through anharmonic coupling with the O−H stretching modes. Note, many of the less intense bands observed in between 750 and 1200 cm^{-1} and not discussed here in detail are also reproduced satisfactorily by the calculations.

III.E. Structural Isomers. In order to understand the discrepancies between experiment and simulation in the C−H stretching region, we searched for structural isomers of **1A**. This search lead to the identification of structures **1B**−**D** (see Scheme 1), which are found only +7, +10, and +15 kJ/mol higher in energy. Compared to the all-trans ground state **1A**, **1B**−**D** differ in the structure of the aliphatic backbone; they all contain a single C−C−C−C unit in cis configuration. The simulated IR spectra of these species are compared to the experimental IRPD spectrum in Figure 5. For a better comparison, the harmonic frequencies were scaled by 0.94 (and not 0.959 as before). The general appearance of the C−H stretch absorption bands is similar, with a few distinctions. Absorption by these isomers can account for some, but not all, of the discrepancies between the experimental IRPD spectra of **1**·Kr and the simulated linear absorption spectrum of **1A** discussed above.

The highest-energy absorption band in the simulated spectrum of **1B** and **1D** is slightly blue shifted, compared to the spectrum of **1A**, which indicates that the shoulder observed at 2940 cm^{-1} may result from absorption of these or even higher-lying conformers. Similarly, the **1B**−**D** also show absorption to the red of the lowest-energy feature in the spectrum of the all-trans conformer **1A**. In particular, the spectrum of **1C** reproduces the lowest observed absorption band at 2925 cm^{-1} satisfactorily. In addition, the simulated spectrum of **1C** can also account for most absorption observed in between the absorption maxima.

Under the experimental conditions (T = 63 K), isolated isomers could either be trapped in local minima or exist as a fluxional system which dynamically interconverts. To better classify the "floppiness" of the ions in our experiment, we calculated the first-order transition states connecting the ground-state structure **1A** with **1B** and **1C**. The MP2/aug-cc-pVDZ energies are 14.6 (**1A**−**1B**) and 12.8 kJ/mol (**1A**−**1C**). Note that even though **1C** lies slightly higher in energy than **1B**, the transition state connecting **1A** and **1C** is slightly lower in energy than the one connecting **1A** and **1B**. In both cases, the barriers to interconversion are small compared to the estimated mean internal vibrational energy of 35 kJ/mol at 63 K. This suggests that dynamically interconverting isomers contribute substantially

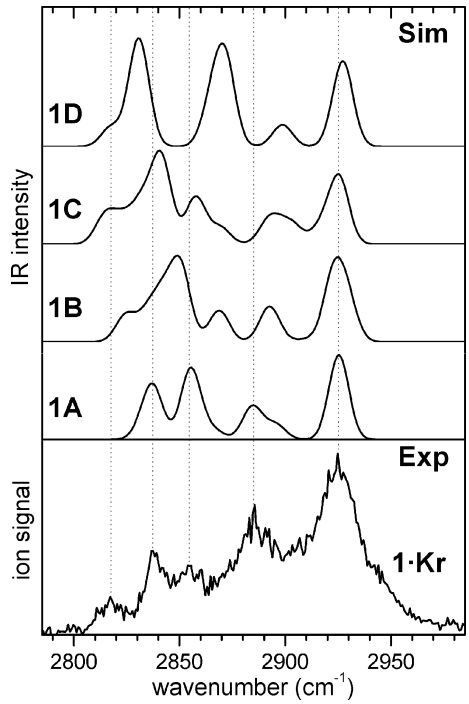

Figure 5. Comparison of the simulated linear absorption spectra of four conformers of **1** (top, traces 1A−1D) and measured IRPD spectrum of **1**·Kr (bottom) in the C−H stretching region. The simulated spectra are derived from MP2/aug-cc-p-VDZ scaled (0.94) harmonic frequencies and intensities, subsequently convoluted using a Gaussian line shape function with a width of 10 cm^{-1} (fwhm).

to the IR absorption spectrum and are the cause of the broadened bands observed in the C−H stretching region.

IV. Conclusions and Outlook

A general strategy for measuring vibrational predissociation spectra of electrosprayed ions has been described, which involves trapping and collisionally cooling these ions under cryogenic conditions in order to drive the entropically unfavorable rare gas atom−ion complex formation process. We have successfully demonstrated that this technique can be used to investigate the vibrational spectra of suberate dianions via the formation of the corresponding Kr atom complexes. The Kr atom binds to one of the carboxylate groups. Its influence on the aliphatic backbone structure is negligible. Ab initio calculations suggest that low barriers to cis−trans isomerization are responsible for the broadening of the spectral features in the C−H stretching region. We find that a single water molecule binds to only one of the two carboxylate groups and in a bidentate fashion. As a result of strong anharmonic coupling, this binding motif yields a very broad band in the O−H stretching region and no noticeable changes on the C−H stretching modes. Addition of up to two water molecules also only has minor effects on the C−C backbone structure.

In order to study the isomerization process at lower temperature, weaker bound rare gas atoms need to be used, which can be formed by lowering the ion trap temperature and increasing the buffer gas pressure. Alternatively, we are interested in studying the effects of microhydration on the structure of **1**. Recent photoelectron studies of these clusters have indicated that a folding transition occurs at elevated temperatures for the **1**·$(H_2O)_{14}$ cluster.[26] Such a transition should yield several characteristic changes in the vibrational spectrum. (i) The folded carbon backbone leads to a significant red shift of the C−H absorption band. (ii) In the folded molecule, the distance between the carboxylate groups is decreased. Consequently, their interaction will be increased, which is directly reflected in the intensity and position of the four carboxylate stretching transitions. (iii) Significant conformation changes should also lead to changes in the hydrogen-bonded network, which is characterized by transitions in the O−H stretching (>3000 cm^{-1}), H−O−H bending (1500−1800 cm^{-1}), and the intermolecular water−ion modes (<1000 cm^{-1}).

Acknowledgment. We gratefully acknowledge the support of the Stichting voor Fundamenteel Onderzoek der Materie (FOM) in providing the required beam time on FELIX and highly appreciate the skillful assistance of the FELIX staff.

References and Notes

(1) Okumura, M.; Yeh, L. I.; Lee, Y. T. *J. Chem. Phys.* **1985**, *83*, 3705.
(2) Bagratashvili, V. N.; Letokhov, V. S.; Makarov, A. A.; Ryabov, E. A. *Multiple Photon Infrared Laser Photophysics and Photochemistry*; Harwood Academic Publishers GmbH: Amsterdam, The Netherlands, 1985.
(3) Lisy, J. M. *Int. Rev. Phys. Chem.* **1997**, *16*, 267.
(4) von Helden, G.; Holleman, I.; Knippels, G. M. H.; van der Meer, A. F. G.; Meijer, G. *Phys. Rev. Lett.* **1997**, *79*, 5234.
(5) Bieske, E. J.; Dopfer, O. *Chem. Rev.* **2000**, *100*, 3963.
(6) Duncan, M. A. *Int. Rev. Phys. Chem.* **2003**, *22*, 407.
(7) Lemaire, J.; Boissel, P.; Heninger, M.; Mauclaire, G.; Bellec, G.; Mestdagh, H.; Simon, A.; Caer, S.; Ortega, J. M.; Glotin, F.; Maitre, P. *Phys. Rev. Lett.* **2002**, *89*, 273002.
(8) Oomens, J.; Sartakov, B. G.; Meijer, G.; Von Helden, G. *Int. J. Mass. Spectrom.* **2006**, *254*, 1.
(9) Asmis, K. R.; Fielicke, A.; von Helden, G.; Meijer, G. Vibrational Spectroscopy of Gas-Phase Clusters and Complexes. In *The Chemical Physics of Solid Surfaces. Atomic Clusters: From Gas Phase to Deposited*; Woodruff, D. P., Ed.; Elsevier: Amsterdam, The Netherlands, 2007; Vol. 12; p 327.
(10) Bosenberg, W. R.; Guyer, D. R. *J. Opt. Soc. Am. B* **1993**, *10*, 1716.
(11) Gerhards, M. *Opt. Commun.* **2004**, *241*, 493.
(12) Johnson, M. A. Vibrational Predissociation Ion Spectroscopy. In *The Encyclopedia of Mass Spectrometry: Theory and Ion Chemistry*; Armentrout, P. B., Gross, M. L., Caprioli, R., Eds.; Elsevier: Oxford, U.K., 2003; Vol. 1.
(13) Kamariotis, A.; Boyarkin, O. V.; Mercier, S. R.; Beck, R. D.; Bush, M. F.; Williams, E. R.; Rizzo, T. R. *J. Am. Chem. Soc.* **2006**, *128*, 905.
(14) Bush, M. F.; Saykally, R. J.; Williams, E. R. *J. Am. Chem. Soc.* **2007**, *129*, 2220.
(15) Brümmer, M.; Kaposta, C.; Santambrogio, G.; Asmis, K. R. *J. Chem. Phys.* **2003**, *119*, 12700.
(16) Santambrogio, G.; Janssens, E.; Li, S.; Siebert, T.; Meijer, G.; Asmis, K. R.; Döbler, J.; Sierka, M.; Sauer, J. *J. Am. Chem. Soc.* **2008**, in press.
(17) Yang, X.; Fu, Y. J.; Wang, X. B.; Slavicek, P.; Mucha, M.; Jungwirth, P.; Wang, L. S. *J. Am. Chem. Soc.* **2004**, *126*, 876.
(18) Oepts, D.; van der Meer, A. F. G.; van Amersfoort, P. W. *Infrared Phys. Technol.* **1995**, *36*, 297.
(19) Frisch, M. J.; Trucks, G. W.; Schlegel, H. B.; Scuseria, G. E.; Robb, M. A.; Cheeseman, J. R.; Montgomery, J. A., Jr.; Vreven, T.; Kudin, K. N.; Burant, J. C.; Millam, J. M.; Iyengar, S. S.; Tomasi, J.; Barone, V.; Mennucci, B.; Cossi, M.; Scalmani, G.; Rega, N.; Petersson, G. A.; Nakatsuji, H.; Hada, M.; Ehara, M.; Toyota, K.; Fukuda, R.; Hasegawa, J.; Ishida, M.; Nakajima, T.; Honda, Y.; Kitao, O.; Nakai, H.; Klene, M.; Li, X.; Knox, J. E.; Hratchian, H. P.; Cross, J. B.; Bakken, V.; Adamo, C.; Jaramillo, J.; Gomperts, R.; Stratmann, R. E.; Yazyev, O.; Austin, A. J.; Cammi, R.; Pomelli, C.; Ochterski, J. W.; Ayala, P. Y.; Morokuma, K.; Voth, G. A.; Salvador, P.; Dannenberg, J. J.; Zakrzewski, V. G.; Dapprich, S.; Daniels, A. D.; Strain, M. C.; Farkas, O.; Malick, D. K.; Rabuck, A. D.; Raghavachari, K.; Foresman, J. B.; Ortiz, J. V.; Cui, Q.; Baboul, A. G.; Clifford, S.; Cioslowski, J.; Stefanov, B. B.; Liu, G.; Liashenko, A.; Piskorz, P.; Komaromi, I.; Martin, R. L.; Fox, D. J.; Keith, T.; Al-Laham, M. A.; Peng, C. Y.; Nanayakkara, A.; Challacombe, M.; Gill, P. M. W.; Johnson, B.; Chen, W.; Wong, M. W.; Gonzalez, C.; Pople, J. A. *Gaussian 03*, revision C.02; Gaussian, Inc.: Wallingford, CT, 2004.
(20) Johnson, R. D., III, Ed. NIST Computational Chemistry Comparison and Benchmark Database, NIST Standard Reference Database Number 101; http://srdata.nist.gov/cccbdb (Released Sept 14, 2006).
(21) Myshakin, E. M.; Jordan, K. D.; Sibert, E. L.; Johnson, M. A. *J. Chem. Phys.* **2003**, *119*, 10138.
(22) Robertson, W. H.; Price, E. A.; Weber, J. M.; Shin, J. W.; Weddle, G. H.; Johnson, M. A. *J. Phys. Chem. A* **2003**, *107*, 6527.

(23) Hesse, M.; Meier, H.; Zeeh, B. *Spektroskopische Methoden in der organischen Chemie*; Georg Thieme Verlag: Stuttgart, Germany, 1987.

(24) Shimanouchi, T. *Tables of Molecular Vibrational Frequencies, Consolidated*; National Bureau of Standards: Washington, DC, 1972; Vol. 1.

(25) Elliott, B. M.; Relph, R. A.; Roscioli, J. R.; Bopp, J. C.; Gardenier, G. H.; Guasco, T. L.; Johnson, M. A. *J. Chem. Phys.* **2008**, 129.

(26) Wang, X. B.; Yang, J.; Wang, L. S. *J. Phys. Chem. A* **2008**, *112*, 172.

JP809390X